Supporting Information

Charge Carrier Dynamics in $Cs_2AgBiBr_6$ Double Perovskites

Davide Bartesaghi[a,b,*], *Adam H. Slavney*[c], *María C. Gélvez-Rueda*[a], *Bridget A. Connor*[c], *Ferdinand C. Grozema*[a], *Hemamala I. Karunadasa*[c], *and Tom J. Savenije* [a,*]

[a] Department of Chemical Engineering, Delft University of Technology, 2628CD Delft, The Netherlands

[b] Materials Innovation Institute (M2i), 2628CD Delft, The Netherlands

[c] Department of Chemistry, Stanford University, Stanford, California 94305, United States

Corresponding Author

*d.bartesaghi@tudelft.nl, t.j.savenije@tudelft.nl

Tel: 0031(0)152783460 (Davide Bartesaghi), 0031(0)152786537 (Tom J. Savenije)

Equilibrium distribution of electrons and holes

The ratio of the number of free charges to the total number of charges shown in Figure 5b in the main text has been calculated assuming thermal equilibrium and using the Boltzmann approximation for the Fermi distributions of electrons and holes,[1] under the assumptions that the Fermi level lies close to the center of the bandgap and that the trap levels for electrons and holes are shallow. The expressions for calculating the equilibrium distribution of holes and electrons are, respectively:

$$\frac{p_0}{p_0+p_T} = \frac{\frac{N_v}{2N_{tp}}\exp\left(-\frac{E_{tp}-E_v}{k_BT}\right)}{1+\frac{N_v}{2N_{tp}}\exp\left(-\frac{E_{tp}-E_v}{k_BT}\right)}, \quad \text{(S1)}$$

$$\frac{n_0}{n_0+n_T} = \frac{\frac{N_c}{2N_{tn}}\exp\left(-\frac{E_c-E_{tn}}{k_BT}\right)}{1+\frac{N_c}{2N_{tn}}\exp\left(-\frac{E_c-E_{tn}}{k_BT}\right)}, \quad \text{(S2)}$$

where p_0 *and* n_0 are the density of free holes and electron, p_T and n_T are the density of trapped holes and electrons, $N_{v(c)}$ is the effective density of states in the valence (conduction) band, $N_{tp(tn)}$ is the density of hole- (electron-) trapping states, $E_{v(c)}$ is the energy level of the valence (conduction) band, $E_{tp(tn)}$ is the energy level of the hole- (electron-) trapping states, k_B is the Boltzmann's constant and T is the absolute temperature.

The effective densities of states in the valence and conduction band are calculated according to

$$N_v = 2\left(\frac{2\pi m_p^* k_B T}{h^2}\right)^{3/2} \quad \text{(S3)}$$

and

$$N_c = 2\left(\frac{2\pi m_n^* k_B T}{h^2}\right)^{3/2}, \quad \text{(S4)}$$

where h is the Planck's constant and $m_p{}^*$ and $m_n{}^*$ are the effective masses of holes and electrons, respectively.

The values of trap densities, of the energy differences between the trapping levels and the band edges, and of the effective masses used for calculating the lines plotted in Figure 5b are reported in table S1.

holes	
N_{tp} (cm^{-3})	3.0×10^{16}
E_{tp} - E_v (eV)	0.13
m_p^{*2}	0.35
Electrons	
N_{tn} (cm^{-3})	2.0×10^{16}
$E_c - E_{tn}$ (eV)	0.11
m_n^{*2}	0.30

Table S1. Parameters used for the calculations of the solid lines in Figure 5b in the main text using Equation S1 and S2. The effective masses of holes and electrons are reported in units of electron mass.

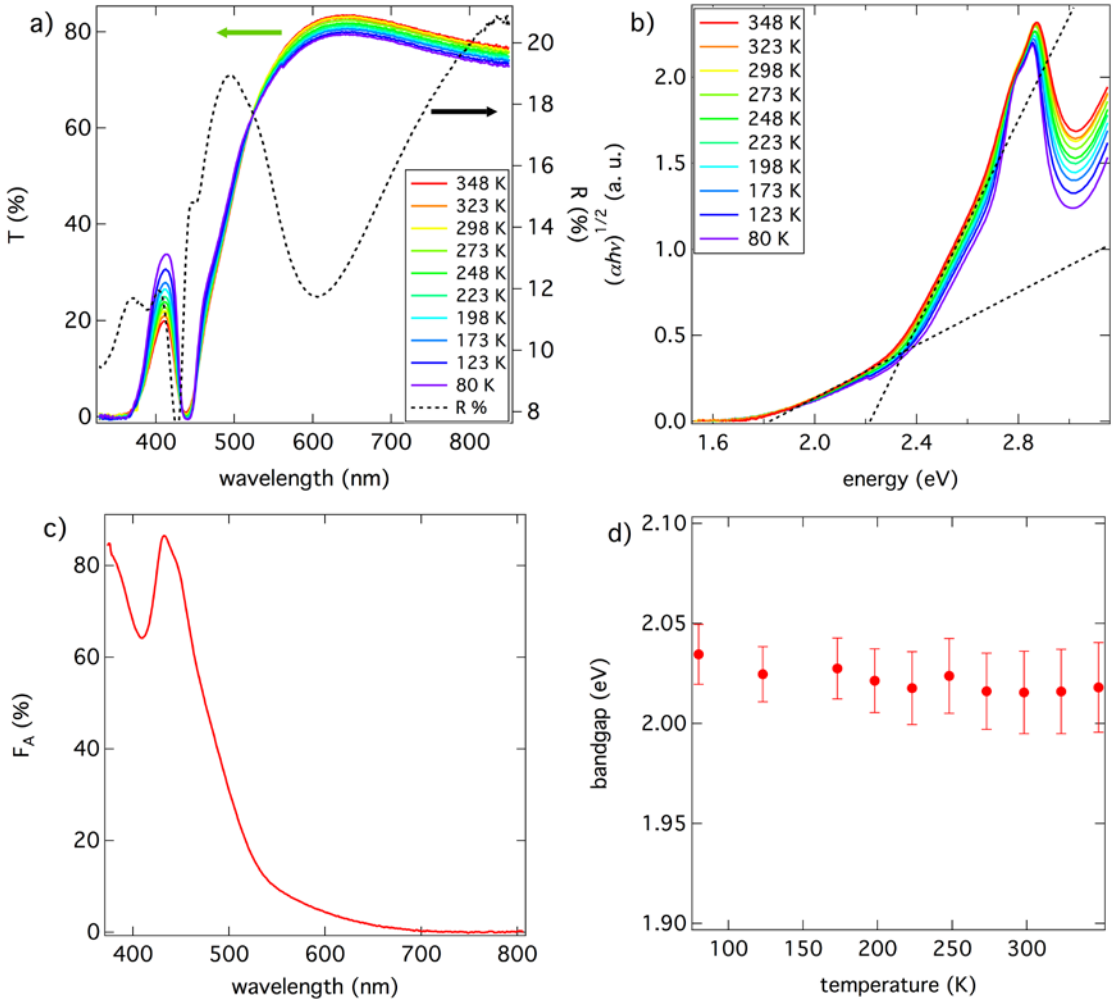

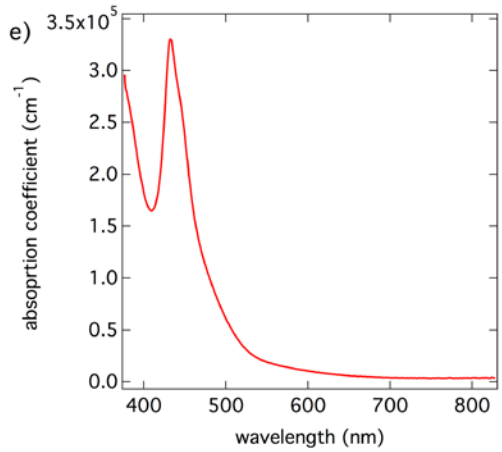

Figure S1. a) Temperature dependent transmittance (colored solid lines) and room temperature reflectance (black dashed line) of the $Cs_2AgBiBr_6$ thin film; b) Tauc plot calculated assuming indirect allowed transition. The linear regions at lower and higher energy correspond to photon absorption assisted by the absorption or the emission of a phonon, respectively. The fit of these regions for the room temperature data is represented by black dashed lines. The bandgap is the midpoint between the two *x*-intercepts of the linear regions; c) fraction of absorbed photons measured at room temperature for the $Cs_2AgBiBr_6$ thin film characterized by means of TRMC measurement in this paper; d) temperature dependent bandgap of $Cs_2AgBiBr_6$ obtained from the fit of the linear regions of the Tauc plot; e) absorption coefficient measured at room temperature for the same sample.

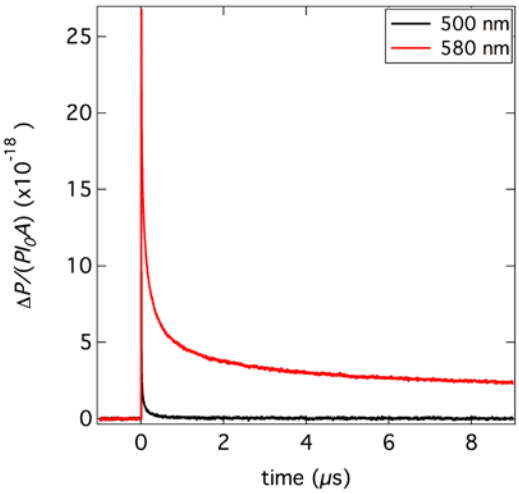

Figure S2. TRMC traces at room temperature for $Cs_2AgBiBr_6$ crystals recorded upon pulsed laser excitation at 500 (black) and 580 nm (red). The fraction of absorbed microwave power $\Delta P/P$ is normalized for the number of incident photons ($I_0 \approx 2.5 \times 10^{15}$ cm^{-2}) and for the surface area of the sample ($A \approx 0.12$ cm^2).

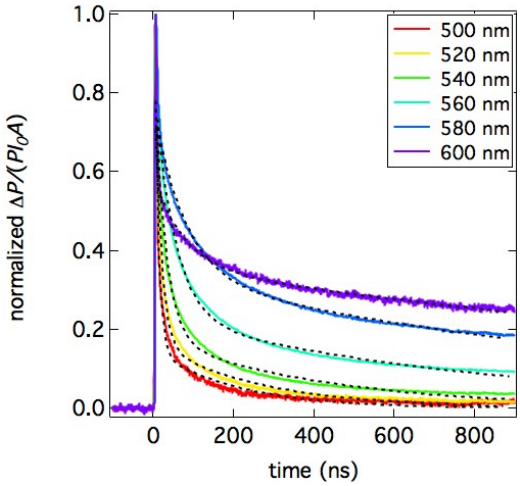

Figure S3. TRMC traces at room temperature for $Cs_2AgBiBr_6$ crystals recorded upon pulsed laser excitation with wavelength in the range 500 – 600 nm. The fraction of absorbed microwave power $\Delta P/P$ is normalized for the number of incident photons ($I_0 \approx 1.1 \times 10^{15}$ cm^{-2}) and for the surface area of the sample ($A \approx 0.12$ cm^2). Subsequently, the signals are normalized to their peak values. The dashed lines represent the double exponential fitting of the experimental data.

Excitation wavelength (nm)	A_f	τ_f **(s)**	A_s	τ_s **(s)**
500	1.327 ± 0.016	(9.520 ± 0.004) × 10^{-9}	0.149 ± 0.001	(2.1 ± 0.5) × 10^{-7}
520	0.907 ± 0.008	(1.580 ± 0.001) × 10^{-8}	0.169 ± 0.001	(2.6 ± 0.4) × 10^{-7}
540	0.739 ± 0.004	(2.800 ± 0.001) × 10^{-8}	0.182 ± 0.001	(4.2 ± 0.5) × 10^{-7}
560	0.624 ± 0.002	(5.050 ± 0.002) × 10^{-8}	0.233 ± 0.001	(8.4 ± 0.9) × 10^{-7}
580	0.440 ± 0.001	(7.690 ± 0.003) × 10^{-8}	0.337 ± 0.001	(1.4 ± 0.5) × 10^{-6}
600	0.232 ± 0.001	(7.69 ± 0.08) × 10^{-8}	0.360 ± 0.001	(2.28 ± 0.02) × 10^{-6}

Table S2. Fit parameters for the double exponential fitting of the TRMC traces shown in Figure S3.

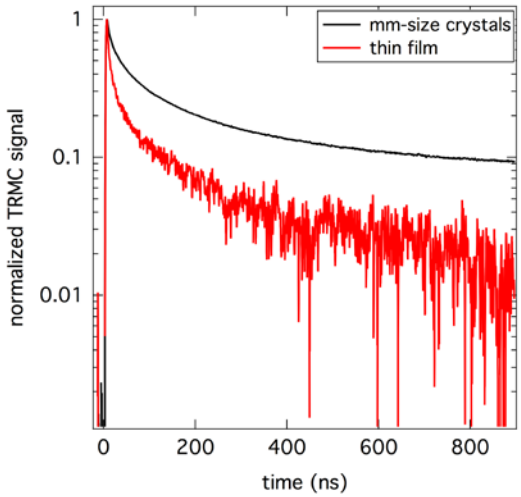

Figure S4: Normalized TRMC signal collected upon optical excitation at 560 nm and photon fluence $I_0 \approx 2.0 \times 10^{15}$ cm^{-2} for $Cs_2AgBiBr_6$ crystals and thin film

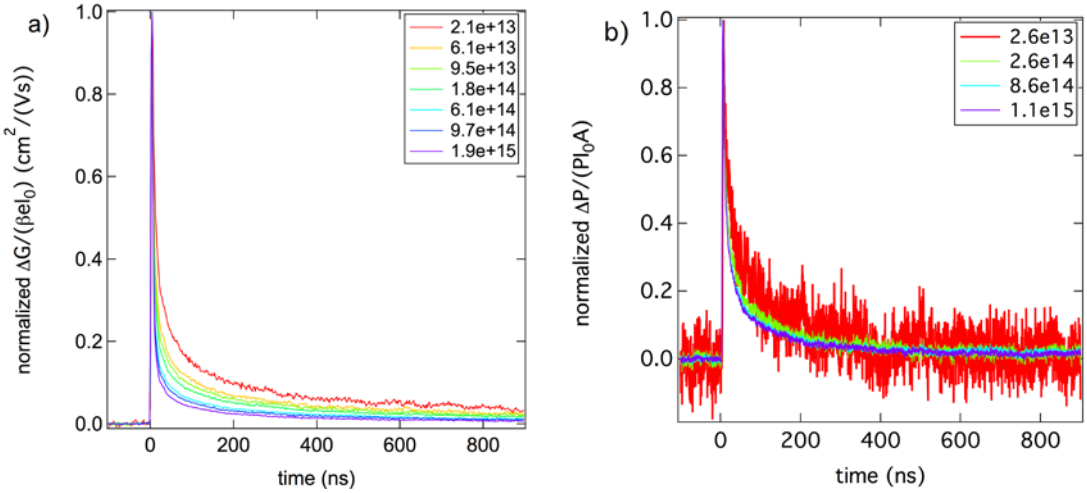

Figure S5: normalized TRMC traces recorded at different photon fluence for $Cs_2AgBiBr_6$ thin film (a) and single crystals (b) upon pulsed laser excitation (λ = 500 nm). The values of the photon fluence in the legends are expressed in photons/cm^2.

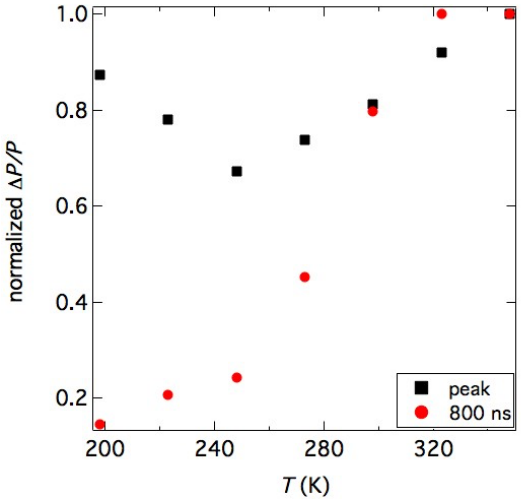

Figure S6: Maximum TRMC signal (black squares) and change in microwave power 800 ns after the laser pulse (red circles) recorded upon optical excitation at 580 nm at different temperatures. The fraction of absorbed microwave power $\Delta P/P$ is normalized for the highest value measured.

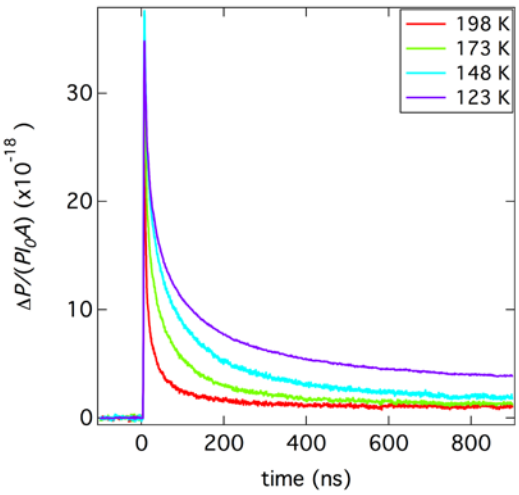

Figure S7: TRMC traces for $Cs_2AgBiBr_6$ crystals recorded upon pulsed laser excitation at 580 nm at temperatures below 198 K. The fraction of absorbed microwave power $\Delta P/P$ is normalized for the number of incident photons ($I_0 \approx 1.1 \times 10^{15}$ cm^{-2}) and for the surface area of the sample ($A \approx 0.12$ cm^2).

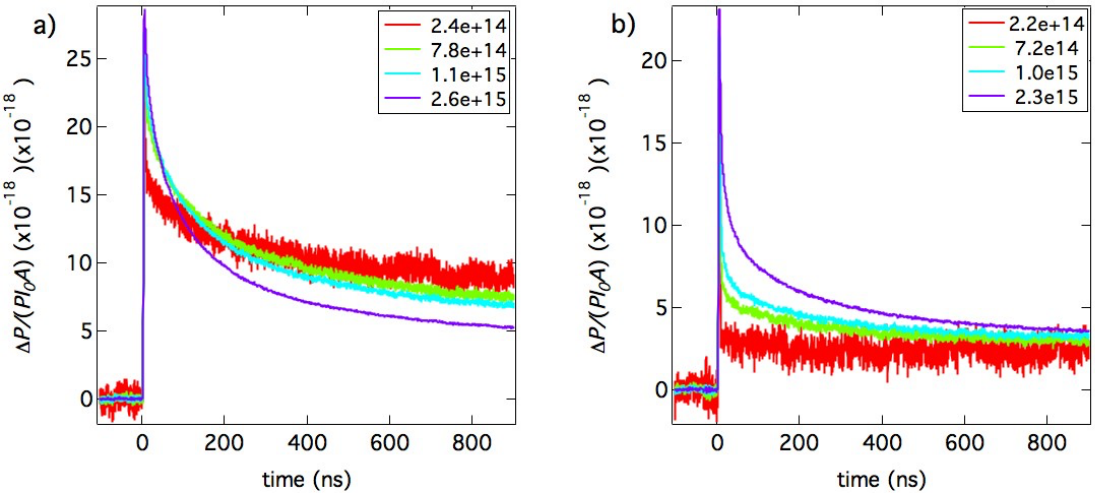

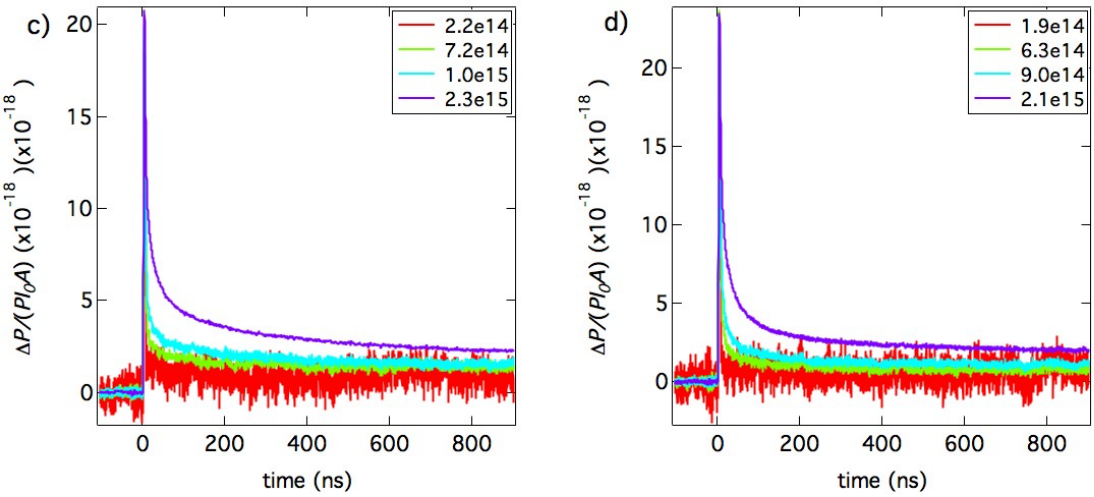

Figure S8: TRMC traces recorded at different photon fluence for $Cs_2AgBiBr_6$ single crystals upon pulsed laser excitation (λ = 580 nm) at 323 K (a), 273 K (b), 248 K (c) and 223 K (d). The values of the photon fluence in the legends are expressed in photons/cm^2.

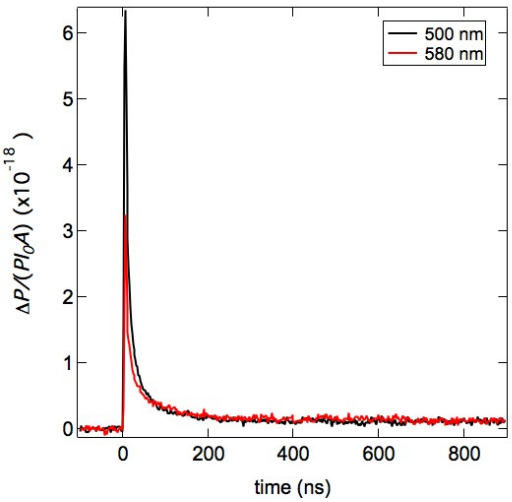

Figure S9: TRMC traces at room temperature for $Cs_2AgBiBr_6$ powder recorded upon pulsed laser excitation at 500 (black) and 580 nm (red). The fraction of absorbed microwave power $\Delta P/P$ is normalized for the number of incident photons ($I_0 \approx 2.5 \times 10^{15}$ cm^{-2}) and for the surface area of the sample ($A \approx 0.12$ cm^2).

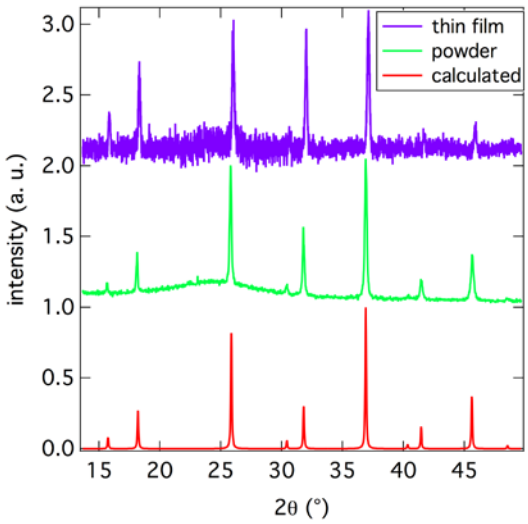

Figure S10: XRD patterns measured for $Cs_2AgBiBr_6$ powder and thin film, and the calculated pattern using the x-ray crystallographic data from Ref. S3.

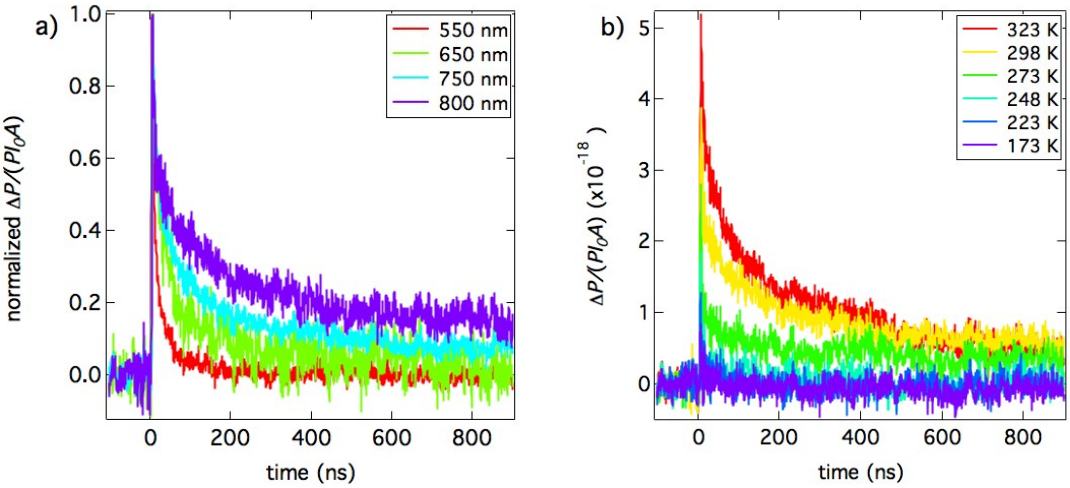

Figure S11: a) TRMC traces at room temperature for $Cs_2(Ag_{1-a}Bi_{1-b})Tl_xBr_6$ ($x = a + b = 0.075$) crystals recorded upon pulsed laser excitation at wavelengths in the range 550 nm – 800 nm; b) TRMC traces recorded for $Cs_2(Ag_{1-a}Bi_{1-b})Tl_xBr_6$ crystals at different temperatures upon excitation at 800 nm. The fraction of absorbed microwave power $\Delta P/P$ is normalized for the number of incident photons ($I_0 \approx 2.5 \times 10^{15}$ cm^{-2}) and for the surface area of the sample ($A \approx 0.12$ cm^2).

REFERENCES

1) Neamen, D. A.; *Semiconductor Physics and Devices: Basic Principles, Fourth Edition*, McGraw-Hill Education, New York 2012.

2) Volonakis, G.; Filip, M. R.; Haghighirad, A. A.; Sakai, N.; Wenger, B.; Snaith, H. J.; Giustino, F. Lead-Free Halide Double Perovskites via Heterovalent Substitution of Noble Metals. *J. Phys. Chem. Lett*. **2016**, *7*, 1254-1259.